Charge-mediated influence of the antibody variable domain on FcRn-dependent pharmacokinetics

Angela Schoch[a], Hubert Kettenberger[b], Olaf Mundigl[c], Gerhard Winter[d], Julia Engert[d], Julia Heinrich[a], and Thomas Emrich[a,1]

[a]Large Molecule Bioanalytical Research and Development, Pharmaceutical Sciences, [b]Large Molecule Research Biochemical and Analytical Research, Large Molecule Research, and [c]Large Molecule Research Discovery, Large Molecule Research, Roche Pharmaceutical Research and Early Development, Roche Innovation Center Penzberg, 82377 Penzberg, Germany; and [d]Institute of Pharmaceutical Technology and Biopharmaceutics, Ludwig Maximilians University, 81377 Munich, Germany

Here, we investigated the influence of the variable fragment (Fv) of IgG antibodies on the binding to the neonatal Fc receptor (FcRn) as well as on FcRn-dependent pharmacokinetics (PK). FcRn plays a key role in IgG homeostasis, and specific manipulation in the crystallizable fragment (Fc) is known to affect FcRn-dependent PK. Although the influence of the antigen-binding fragment (Fab) on FcRn interactions has been reported, the underlying mechanism is hitherto only poorly understood. Therefore, we analyzed the two IgG1 antibodies, briakinumab and ustekinumab, that have similar Fc parts but different terminal half-lives in human and systematically engineered variants of them with cross-over exchanges and varied charge distribution. Using FcRn affinity chromatography, molecular dynamics simulation, and in vivo PK studies in human FcRn transgenic mice, we provide evidence that the charge distribution on the Fv domain is involved in excessive FcRn binding. This excessive binding prevents efficient FcRn–IgG dissociation at physiological pH, thereby reducing FcRn-dependent terminal half-lives. Furthermore, we observed a linear correlation between FcRn column retention times of the antibody variants and the terminal half-lives in vivo. Taken together, our study contributes to a better understanding of the FcRn–IgG interaction, and it could also provide profound potential in FcRn-dependent antibody engineering of the variable Fab region.

FcRn | pharmacokinetics | antibody | charge | engineering

Human IgGs contain two antigen-binding (Fab) regions that convey specificity for the target antigen and a constant (Fc) region that is responsible for interactions with Fc receptors (1, 2). Human IgGs of subclasses 1, 2, and 4 have an average serum half-life of 21 days (d), which is longer than that of any other known serum protein (3). This long half-life is predominantly mediated by the interaction with the neonatal Fc receptor (FcRn) (4, 5) and is one of the reasons why IgGs or Fc-containing fusion proteins are widely used as therapeutic proteins.

FcRn is a membrane-associated receptor involved in both IgG and albumin homeostasis, in maternal IgG transport across the placenta, and in antigen–IgG immune complex phagocytosis (6–8). Human FcRn is a heterodimer consisting of the glycosylated class I major histocompatibility complex-like protein (α-FcRn) and a β_2 microglobulin (β_2m) subunit (9). FcRn binds to a site in the C_H2-C_H3 region of the Fc region (10–13), and two FcRn molecules can bind to the Fc region simultaneously (14, 15). The affinity between FcRn and Fc is strongly pH dependent, showing nanomolar affinity at endosomal pH of 5–6 and negligible binding at a physiological pH of 7.4 (12, 16, 17). The underlying mechanism conveying long half-life to IgGs can be explained by three fundamental steps. First, IgGs are subject to unspecific pinocytosis by various cell types (18, 19). Second, IgGs encounter and bind FcRn in the acidic endosome at a pH of 5–6, thereby protecting IgGs from lysosomal degradation (10, 17, 20). Finally, IgGs are released in the extracellular space at physiological pH of 7.4 (4). This strict, pH-dependent bind-and-release mechanism is critical for IgG recycling, and any deviation of the binding

characteristics at different pHs may strongly influence circulation half-lives of IgGs (21).

In addition to the specific interaction of the Fc region with FcRn, the Fab regions have also been suggested to contribute to FcRn binding (22–24). For example, Fab-mediated residual binding at near physiological pH was correlated with the pharmacokinetic properties of a set of therapeutic antibodies, indicating that IgGs with excessive binding to FcRn at pH 7.3 suffer from reduced terminal half-lives (23). Recently, Schlothauer et al. (24) have described a novel pH gradient FcRn affinity chromatography method that closely mimics physiological conditions for the dissociation between FcRn and IgGs. Furthermore, they showed that IgGs with identical Fc regions differ in their dissociation from FcRn, thereby indicating the influence of the Fab region on FcRn binding. However, the underlying mechanism how the distal Fab region influences FcRn binding is hitherto only poorly understood.

To systematically investigate the influencing factors of the Fab region to FcRn-mediated IgG homeostasis, we used the antibody pair briakinumab (Ozespa) and ustekinumab (Stelara) as a model system. Both briakinumab and ustekinumab are fully human monoclonal IgG1 antibodies that specifically bind to the human p40-subunit of interleukin 12 and interleukin 23 (25) and not to the corresponding mouse interleukin 12 and interleukin 23. Both antibodies have nearly identical constant IgG1 domains, with minor differences in several allotype-specific amino acids in this region (Fig. S1). However, these different amino acids are outside of the cognate FcRn-binding regions and therefore are considered to play no significant role in FcRn-dependent

Significance

Therapeutic antibodies of the immunoglobulin G (IgG) isotype show a pharmacokinetic (PK) profile that is strongly mediated by the interaction with the neonatal Fc receptor (FcRn). Therefore, modulating the FcRn–IgG interaction allows altering PK characteristics of therapeutic antibodies. So far, engineering the crystallizable fragment (Fc) is known to affect PK, and, although the influence of the antigen binding fragment (Fab) on FcRn interactions has been reported, the underlying mechanism remains unknown. Here, we demonstrate that the charge distribution in the distal variable fragment (Fv) of IgGs is involved in excessive binding to the FcRn, thereby reducing FcRn-dependent terminal half-lives in vivo. These findings contribute to a better understanding of the FcRn–IgG interaction.

pharmacokinetics (PK) (10). Briakinumab is an IgG1$_\lambda$ antibody with variable heavy and light chain domains of the V$_H$3 and V$_\lambda$1 germ-line families. Ustekinumab is an IgG1$_\kappa$ antibody with variable heavy and light chain domains of the V$_H$5 and V$_\kappa$1D germ-line families. Interestingly, ustekinumab has a median terminal half-life of 22 d (26) whereas briakinumab has a terminal half-life of only 8–9 d (25, 27, 28). Therefore, we used briakinumab and ustekinumab as our model system to elucidate the role of the Fab region on FcRn-dependent PK.

Here, we report that the charge distribution in the variable fragment (Fv) domain is involved in excessive FcRn binding, thereby reducing FcRn-dependent terminal half-lives. To elucidate which structural element of the Fab region and how the Fab region influences FcRn binding, we engineered nine variants of briakinumab and ustekinumab. Furthermore, we analyzed all 11 antibodies using a combination of in vitro FcRn affinity chromatography, molecular dynamics (MD) simulation, subcellular trafficking analysis by confocal microscopy, and in vivo PK studies in human FcRn transgenic mice.

Results

Charge Distribution and pH-Dependent Net Charge. Using the published crystal structure of ustekinumab (29) and a homology model of briakinumab, we observed that briakinumab exhibits an unusual, nonuniform charge distribution at physiological pH of 7.4. Briakinumab shows a large positively charged region on the Fv domain (Fig. 1A) that is absent in ustekinumab (Fig. 1B). Furthermore FcRn was found to possess an extended negatively charged region (Fig. 1C) that is, however, not involved in cognate Fc binding. Briakinumab and ustekinumab have a similar isoelectric point of 9.6 and 9.3, respectively, whereas the net charge of briakinumab is slightly more positive over the entire pH range (Fig. 1D) than the net charge of ustekinumab. Therefore, we hypothesized that the FcRn–Fv interaction could be charge-mediated.

pH-Dependent FcRn–IgG Interaction. To investigate whether the reduced terminal half-life of briakinumab is caused by an altered binding to FcRn involving the positively (briakinumab) and negatively (FcRn) charged regions, we constructed nine variants of briakinumab and ustekinumab (Table 1). In particular, we systematically modified the variable regions and tested their influence on FcRn binding at pH 6.0 and on FcRn dissociation using surface plasmon resonance (SPR) and FcRn affinity chromatography (Table 2), respectively.

The FcRn affinities at pH 6.0 fell in a narrow range for all 11 antibodies (Table 2). The equilibrium dissociation constant (K_D) was calculated relative to ustekinumab (ustekinumab = 1.0). Briakinumab had a relative K_D of 0.2, and the nine variants ranged between briakinumab and ustekinumab. Due to this rather small K_D difference, we concluded that different terminal half-lives are not caused by different FcRn binding at pH 6.0.

To mimic the FcRn–IgG dissociation at physiological pH, we analyzed the elution profiles of the 11 antibodies using an FcRn affinity column with pH gradient elution (Fig. 2). Ustekinumab and mAb 1, which bears the Fv domain of ustekinumab on the constant parts of briakinumab, showed indistinguishable retention times at around 84 min, indicating that the Fv domain influences the interaction with the FcRn. Briakinumab, on the other hand, eluted at a retention time of 94 min and therefore showed a clear difference in retention time compared with ustekinumab. The indistinguishable retention times of the immunoglobulin G-degrading enzyme of *Streptococcus pyogenes* (IdeS)-cleaved Fc regions of briakinumab (85.7 min) and ustekinumab (85.2 min) supported the negligible role of the Fc region in this setting. The mAb 4 containing ustekinumab light chains (LCs) and briakinumab heavy chains (HCs) eluted close to ustekinumab, revealing the impact of the LC on FcRn binding in this model system. To study the influence of the complementarity-determining regions (CDRs) on FcRn dissociation, we constructed variants mAb 5 and mAb 6 that bear ustekinumab CDRs on the briakinumab framework and vice versa. Grafting ustekinumab
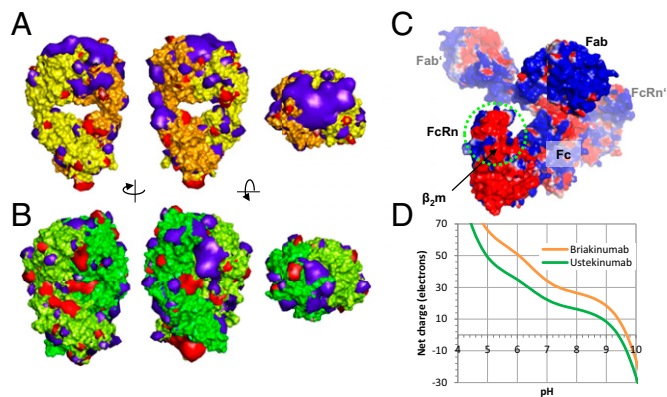

Fig. 1. Charge distribution and pH-dependent net charge. Isopotential surfaces of the proteins protonated at pH 7.4 and contoured at 2 k$_B$T/e. Blue, positive; red, negative. (A) Briakinumab. The light chain is shown in yellow, and the heavy chain is shown in orange. Views of the *Middle* and *Right* images are related to the view in the *Left* panel by a rotation about a vertical and a horizontal axis, respectively. (B) Ustekinumab. Light and heavy chains are colored in light and dark green, respectively. The views are identical to A. (C) Homology model of briakinumab in complex with two human FcRn/β$_2$ microglobulin (β$_2$m) heterodimers, shown as molecular surface. The surface is colored according to its electrostatic potential (±1 k$_B$T/e) calculated as above. A green circle marks the positive charge patch on FcRn deemed to interact with a negative patch on the Fab. Protein structures were prepared with DiscoveryStudio Pro. (D) Sequence-based calculated net charge vs. pH of briakinumab and ustekinumab.

CDRs on briakinumab (mAb 5) shifted the retention time of mAb 5 close to that of ustekinumab. However, the opposite was not observed to the same extent. Briakinumab CDRs on ustekinumab (mAb 6) described an elution profile that was still close to ustekinumab. A strong retention time shift from briakinumab in the direction of ustekinumab was observed for mAb 9, which is a briakinumab variant in which three positively charged residues in the light chain CDRs were mutated to alanines. Three and five positively charged residues in the heavy chain of briakinumab were mutated in mAb 7 and mAb 8, respectively. Here, the retention time shift relative to briakinumab was not as strong as for mAb 9. The mAb 3, comprising the HCs of ustekinumab and the LCs of briakinumab, as well as mAb 2 containing the Fv domain of briakinumab on the ustekinumab constant domains, both eluted close to briakinumab. Taken together, we showed that the Fv domain influences FcRn dissociation and not FcRn binding at pH 6.0.

To study in more detail the nature of the FcRn–Fv interaction, we tried to correlate the FcRn column retention times with calculated isoelectric points and net charges of the antibodies. We did not observe a correlation between the FcRn column retention times and the isoelectric points or the net charges of the Fv domains at lysosomal pH 6.0 or physiological pH 7.4 (Table 2). However, we observed that the FcRn column retention times increased with the extent of positively charged regions on the Fv structures, especially around the light chain variable domains (Fig. 2). We next measured FcRn column retention times in the presence of increasing salt concentrations because charge-mediated interactions are known to be weakened under high ionic strength conditions. We observed that the FcRn column retention time of briakinumab was shortened in the presence of salt in a manner proportional to the inverse square root of the ionic strength, as suggested by the Debye–Hückel law of charge screening (30). Conversely, the retention time of ustekinumab remained essentially unaffected (Fig. S2). Therefore, we demonstrated that a significant part of the excessive FcRn–briakinumab interaction is charge-mediated.

Correlation Between in Vivo PK Parameters and FcRn Column Elution pHs. To assess whether the effect of mutated charged residues in the variable domains of briakinumab on FcRn binding translates

Table 1. Systematically engineered variants of briakinumab and ustekinumab

Name	Description
Briakinumab	Briakinumab
Ustekinumab	Ustekinumab
mAb 1	Ustekinumab Fv + briakinumab constant domains
mAb 2	Briakinumab Fv + ustekinumab constant domains
mAb 3	Ustekinumab HC + briakinumab LC
mAb 4	Briakinumab HC + ustekinumab LC
mAb 5	Ustekinumab CDRs on briakinumab
mAb 6	Briakinumab CDRs on ustekinumab
mAb 7	Briakinumab R19HCA, K64HCA, R83HCA*
mAb 8	Briakinumab R16HCA, R19HCA, K57HCA, K64HCA R83HCA*
mAb 9	Briakinumab R27LCA, R55LCA, R94LCA*

Structural parts like Fv, LC, and CDRs were exchanged between briakinumab and ustekinumab: mAb 1–6. Three and five basic amino acids in the HC of briakinumab were exchanged into alanines for mAb 7 and mAb 8, respectively. MAb 9 is briakinumab with three basic amino acids in the LC CDRs exchanged into alanines. Asterisks (*) mark exchanged amino acid residues according to the EU numbering of Kabat (45).

into modulated in vivo PK properties, we conducted PK studies in human FcRn transgenic mice. Briakinumab and ustekinumab, together with two variants of briakinumab (mAb 8 and mAb 9), which had FcRn column retention times between briakinumab and ustekinumab, were tested. Mean serum concentration-time profiles for the antibodies are shown in Fig. 3A. As expected, briakinumab and ustekinumab significantly differ in their PK behavior, showing terminal half-lives of 48 h and 137 h, respectively (Fig. 3B). Briakinumab also showed a faster decrease in the α-phase that might be caused by different distribution processes. In our study, the variants mAb 8 and mAb 9, which have smaller positively charged regions in the Fv domain compared with briakinumab, had terminal half-lives of 78 h and 109 h, respectively. A statistical significance could be detected between the terminal half-lives of briakinumab and ustekinumab and of briakinumab and mAb 9, as well as of ustekinumab and mAb 8. Ustekinumab, mAb 9, mAb 8, and briakinumab eluted at 84.3, 86.2, 90.1, and 93.7 min, corresponding to an elution pH of 7.4, 7.5, 7.7, and 7.9, respectively. Importantly, the terminal half-lives of the four IgGs were linearly correlated with the in vitro FcRn column elution pHs (Fig. 3B).

Subcellular Trafficking Analysis. To analyze the influence of the differently charged Fv regions of briakinumab and ustekinumab at the cellular level, we incubated human umbilical vein endothelial cells (HUVECs) with the directly fluorescently labeled IgGs to allow fluid phase pinocytosis under physiological conditions.

Within 40 min of incubation (20-min loading period followed by a 20-min chase period), both briakinumab and ustekinumab could be found in distinct subdomains of FcRn-positive sorting endosomes (17, 31), indicating that the two IgGs are differentially sorted already at this level (Fig. 4).

Molecular Dynamics Simulation of the FcRn–IgG Models. To further support the hypothesis of a charge-mediated Fab–FcRn interaction, we studied the dynamics of the FcRn–IgG complexes by MD simulation. We used the recently published structure of human FcRn in complex with a human Fc and serum albumin (PDB ID code 4N0U). We superimposed this complex (omitting serum albumin) with the crystal structure of a complete IgG1 (PDB ID code 1HZH) and with the X-ray structure of the Fab fragment of ustekinumab (PDB ID code 3HMX). Because no experimental structure of briakinumab was available, we used a homology model instead (*Materials and Methods*). These IgG–FcRn complex models contain two copies of FcRn (α-FcRn with β2m) on one complete IgG molecule (Figs. 1C and 5A). The distance between the FcRn and the Fv domains is ~40 Å in the starting structure and thus exceeds the Debye length of ~8 Å under physiological conditions (30). Consequently, the Fv domain must approach the FcRn to establish an attractive interaction. To study whether conformational flexibility of the IgG1 hinge region supports such domain movements, we calculated the molecular dynamics of the briakinumab and ustekinumab FcRn–IgG complexes over a period of 100 ns in explicit water. During the course of the simulation, one of the two Fab arms of briakinumab approached the tip of FcRn and persisted in this conformation for the rest of the simulation time (Fig. 5 A, B, and D). This finding suggests that the conformational flexibility of the Fab arms allows them to readily assume conformations that can stably interact with FcRn. The region on FcRn found to interact with the Fv domain has not been described as being involved in IgG binding before. In this MD simulation, the Fab arms of ustekinumab did not approach FcRn but randomly moved in conformations without particular preferences. (Fig. 5 A, B, and D). In summary, MD simulation indicates that the flexibility of Fab arms in the FcRn–IgG complexes structurally allows a direct, stabilizing interaction of the Fv domain with the tip of FcRn.

Discussion

Specific manipulation of the Fc region is known to affect PK characteristics by altering the interaction between the Fc region and FcRn, especially at pH 6.0, and has been used to design therapeutic antibodies with specific PK properties (32, 33). Although the influence of the Fab region on FcRn interactions has recently been discussed, when antibodies of the same WT human Fc sequences but different Fab regions showed differences in FcRn binding and altered PK, the underlying mechanism of this interaction remained unclear (22, 23). In this study, we provide

Table 2. FcRn affinities and calculated net charge of all tested antibodies

Name	Ret. time (min)	Rel. K_D	pI (IgG)	q(V_L) pH 6	q(V_L) pH 7.4	q(V_H) pH 6	q(V_H) pH 7.4	q(Fv) pH 6.0	q(Fv) pH 7.4
Ustekinumab	84.3	1	9.3	2.1	1.9	3.1	2.9	5.2	4.9
mAb 1	84.3	1.0 ± 0.22	9.5	2.1	1.9	3.1	2.9	5.2	4.9
mAb 4	84.5	0.5 ± 0.08	9.6	2.1	1.9	6.4	4.3	8.4	6.2
mAb 5	85.1	0.9 ± 0.16	9.9	2.1	1.9	4.1	3.9	6.1	5.9
mAb 6	86.2	0.4 ± 0.17	9.0	3.9	3.0	5.4	3.3	9.2	6.3
mAb 9	86.2	0.4 ± 0.04	9.1	0.8	0.0	6.4	4.3	7.2	4.3
mAb 8	90.1	0.4 ± 0.07	8.8	3.8	3.0	1.4	−0.7	5.2	2.3
mAb 7	90.4	0.2 ± 0.03	9.2	3.8	3.0	3.4	1.3	7.2	4.3
mAb 3	92.4	0.2 ± 0.06	9.3	3.8	3.0	3.1	2.9	6.9	6.0
mAb 2	93.0	0.3 ± 0.19	9.3	3.8	3.0	6.4	4.3	10.2	7.3
Briakinumab	93.7	0.2 ± 0.07	9.6	3.8	3.0	6.4	4.3	10.2	7.3

Antibodies are sorted according to the FcRn column retention times (Ret. time). The equilibrium dissociation constant K_D was calculated as steady-state affinity and normalized to the K_D of ustekinumab. Relative (Rel.) K_D values (ustekinumab = 1) are presented as the mean ($n = 3$) ± SD.
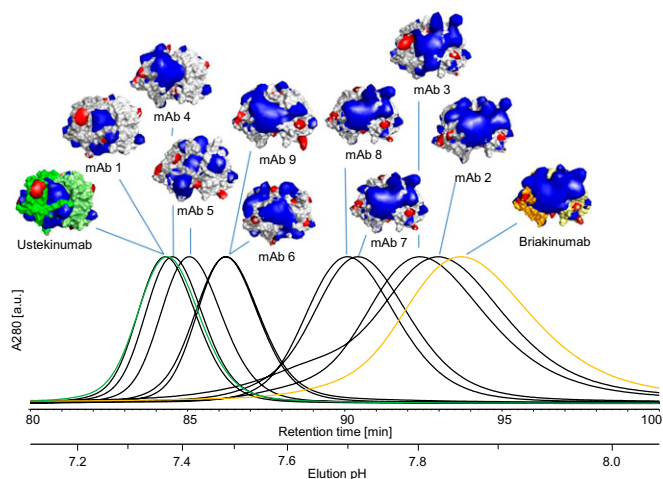
Fig. 2. pH-dependent FcRn–IgG interaction. FcRn affinity chromatograms of the 11 IgG variants were intensity-normalized for clarity. A molecular surface representation of the structural models, protonated at pH 7.4, was superimposed with isopotential surfaces contoured at 2 k_BT/e. The view is identical to the *Right* panel in Fig. 1*A* and focuses on the CDR regions. A second horizontal axis indicates the elution pH, interpolated from offline pH measurements.

evidence that FcRn binding of briakinumab and ustekinumab at pH 6.0 was similar whereas the dissociation from the FcRn was very different. Using variants of briakinumab and ustekinumab, we showed that the interaction is predominantly electrostatic and correlates with the extent of a positively charged region.

FcRn affinity chromatography of the engineered variants showed that antibodies with the same Fv domain (mAb 1 and mAb 2) and the same LC (mAb 3 and mAb 4) elute at nearly identical FcRn column retention times. Furthermore, grafting ustekinumab CDRs on briakinumab (mAb 5) shifts the elution pH close to that of ustekinumab. Combining these results leads to the conclusion that the light chain CDRs provide the main influence on briakinumab's FcRn binding. Grafting briakinumab CDRs on ustekinumab (mAb 6) presented an elution profile that was still close to ustekinumab. We could not fully elucidate the reason for this phenomenon, but the FcRn interaction is probably more affected by disrupting the large positively charged region of briakinumab than by creating a positively charged region that was significantly smaller. As suggested by the MD simulation, a direct, stabilizing interaction between a positively charged Fv region and a negatively charged region on FcRn is readily feasible. Thus, FcRn–Fv interaction may lead to a slower-than-normal dissociation of the FcRn–IgG complex under physiological conditions.

Previous studies have discussed net charge to be a driving force for altered PKs by affecting the electrostatic interaction between the antibody and negatively charged groups on the surface of endothelial cells (34, 35). For example, Igawa et al. (36) observed that IgG4 antibodies with lower isoelectric point (pI) values due to engineering in the variable region have a lower rate of fluid-phase pinocytosis and in turn a reduced elimination rate. Furthermore, Boswell et al. (37) proposed the pI differences needed to be at least of one unit to influence PK. In contrast, the pI values of briakinumab, ustekinumab, and mAb 9 were found to be in a relatively narrow range between 9.3 and 9.6 and the pI of mAb 8 was determined to be 8.8. Therefore, we assume the influence on fluid-phase pinocytosis to be minimal. However, briakinumab's shorter FcRn column retention times under high ionic strength conditions, as well as the higher electrostatic contribution to the FcRn–Fv interaction compared with ustekinumab in the MD simulation, indicated that a specific located charge may be the main influencing factor on the FcRn–IgG interaction. The influence of charge in the Fv domain was analyzed using mutants that have three (mAb 7) and five (mAb 8) positively charged

residues in the HC of briakinumab mutated as well as briakinumab with three positively charged residues mutated in the light chain CDRs (mAb 9). MAb 7 and mAb 8 showed small retention time shifts in the direction of ustekinumab, confirming a charge-mediated interaction, whereas mAb 9 showed a high retention time shift in the direction of ustekinumab. Thus, we conclude that a specific located charge in the light chain CDRs strongly influences FcRn dissociation.

In our in vivo experiments in human FcRn transgenic mice, we focused on the influence of the Fv domain on FcRn recycling; therefore, we examined the terminal half-life, which is exclusively calculated in the elimination phase where FcRn recycling dominates (38). The terminal half-life of the four antibodies correlated linearly with the in vitro FcRn column elution pH, thereby indicating the potential of FcRn affinity chromatography to predict Fab-mediated PK properties. The correlation between terminal half-lives and the FcRn column elution pH confirmed the importance of the efficient FcRn–IgG dissociation at physiological pH. A similar finding has been observed for Fc-engineered IgG molecules with improved FcRn binding at both endosomal pH 6.0 and at physiological pH 7.4, which did not show prolonged half-life (39). The FcRn–IgG complex is built in the endosomes at pH 6.0; therefore, less binding results in less IgG recycling and faster clearance. During exocytosis, the FcRn–IgG complex is released to the plasma membrane, where the dissociation of the IgG and the FcRn has to take place at a physiological pH of 7.4 within a short period (40). Consequently, dissociation at physiological pH is also important for a prolonged half-life (21, 40). In conclusion, our experiment supports the hypothesis that a slower dissociation at higher pH could lead to degradation of the antibodies in the lysosome instead of releasing the antibodies back to blood circulation. In addition, cellular internalization and sorting experiments demonstrate a separation of briakinumab and ustekinumab at the level of the
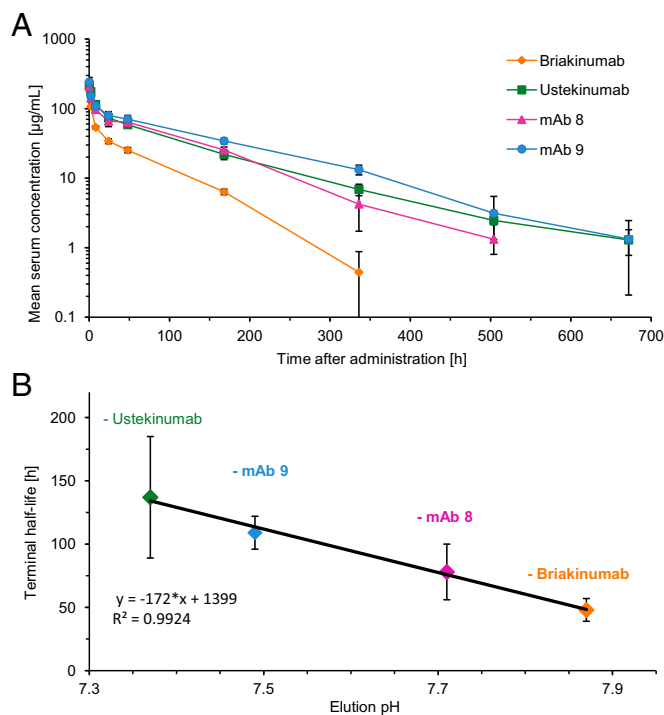

Fig. 3. Correlation between in vivo PK parameters and FcRn column elution pHs. Antibodies were administered as a single i.v. bolus injection of 10 mg/kg to six animals per group. Data points represent the mean ± SD. (*A*) Blood level curves of briakinumab (orange), ustekinumab (green), mAb 8 (purple), and mAb 9 (blue). (*B*) Correlation between the terminal half-lives with the FcRn column elution pH.
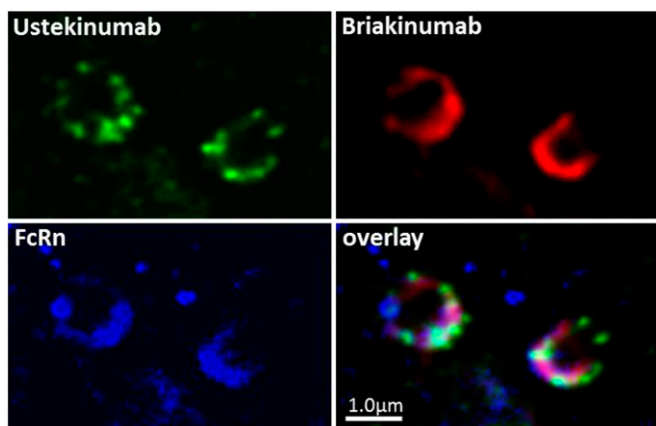
Fig. 4. Differential sorting of briakinumab and ustekinumab in FcRn-positive sorting endosomes. HUVECs were incubated together with 200 µg/mL both briakinumab (labeled with AlexaFluor594) and ustekinumab (labeled with AlexaFluor488) for 20 min at 37 °C, pH 7.3, followed by 20 min chase. At the end of the experiment, cells were fixed and counterstained with a monoclonal antibody directed against FcRn (DVN22) (44) detected by secondary antibodies labeled with AlexaFluor647.

sorting endosome, suggesting that differential sorting appears already at this level. Evidence for the presence of separate recycling pathways originating from the same endosomal compartment has been described previously (31, 41). Gan et al. have also proposed a model of how the subsequent routing of FcRn to lysosomal degradation may occur (42). It would be important to further investigate the separation of IgGs with different charge distributions to either recycling or lysosomal degradation to gain further insight into the sorting steps involved in the differential trafficking (17, 42, 43).

Our results show that charge in the Fv domain of an IgG affects the terminal half-life by altering the interaction between the IgG and FcRn. Furthermore, we not only located the structural parts of the Fab that interact with FcRn but also demonstrated the interaction to be charge-mediated. Finally, the PK study revealed a linear correlation between the in vitro FcRn–IgG dissociation and the terminal half-life in vivo, thereby providing a better understanding of FcRn-dependent PK.

Materials and Methods

Mice. Mouse husbandry was carried out under specific pathogen-free conditions. Mice were obtained from The Jackson Laboratory (female, age 4–10 wk, weight 17–22 g at time of dosing). All animal experiments were approved by the Government of Upper Bavaria, Germany (permit no. 55.2-1-54-2532.2-28-10) and performed in an AAALAC-accredited animal facility according to the European Union Normative for Care and Use of Experimental Animals. The animals were housed in standard cages and had free access to food and water during the whole study period.

Antibodies. The antibodies used in these experiments were briakinumab (ABT 874, J 695, Ozespa, SEQ ID No. 36, PN WO2001014162-A2) and ustekinumab (CNTO 1275, Stelara, CAS Registry No. 815610-63-0), as well as nine mutants of briakinumab and ustekinumab, hereafter referred to as mAb 1 to mAb 9, respectively. In total, 11 IgGs were investigated (Table 1).

FcRn Affinity Chromatography. FcRn affinity columns were prepared as described by Schlothauer et al. (24), and antibodies were eluted by a linear pH gradient from pH 5.5–8.8 within 120 min using 20 mM Mes, 140 mM NaCl, pH 5.5, and 20 mM Tris, 140 mM NaCl, pH 8.8, as eluents. To determine the elution pH at particular retention times, samples were collected every 5 min, and the pH was measured offline.

To investigate the influence of higher salt concentrations, running buffers containing 140 mM, 170 mM, 200 mM, 250 mM, 300 mM, and 400 mM sodium chloride were used.

FcRn Affinity Using Surface Plasmon Resonance Analysis. The steady-state binding levels and the equilibrium dissociation constants (K_D) for human FcRn (huFcRn) and the IgGs were determined at pH 6.0 using a BiaCore T100 SPR instrument (GE Healthcare). Human FcRn was immobilized on a BiaCore CM5-biosensor chip (GE Healthcare Bioscience) via amine coupling to a level of 50 response units (RUs). For mAb 5 and mAb 6, a CM4-biosensor chip was used. The assay was performed using PBS containing 0.05% Tween 20 (both from Roche Diagnostics) adjusted to pH 6.0 as running and dilution buffer at room temperature. A concentration series of the samples was prepared in a range of 1,500 nM to 23 nM, and each sample was injected at a flow rate of 5 µL/min. Association and dissociation times of 600 and 360 s, respectively, were used. The chip was regenerated by injection of PBS containing 0.05% Tween 20 at pH 7.5. The equilibrium dissociation constant K_D was calculated as steady-state affinity and normalized to the K_D of ustekinumab.

Cell Culture and Confocal Immunofluorescence Analysis. HUVECs were grown on calibrated glass coverslips to a confluency of 80%. Subsequently, cells were incubated with 200 µg/mL ustekinumab_AlexaFluor488 and briakinumab_AlexaFluor594 for 20 min at 37 °C, pH 7.3, washed three times, and chased in fresh medium for an additional 20 min before fixation. Antibodies were directly labeled according to the manufacturer's instructions (Life Technologies). FcRn binding was quality controlled by SPR analysis. Cells were then counterstained with anti-FcRn monoclonal antibody DVN22 (44), followed by anti-mouse secondary antibodies conjugated to AlexaFluor647.
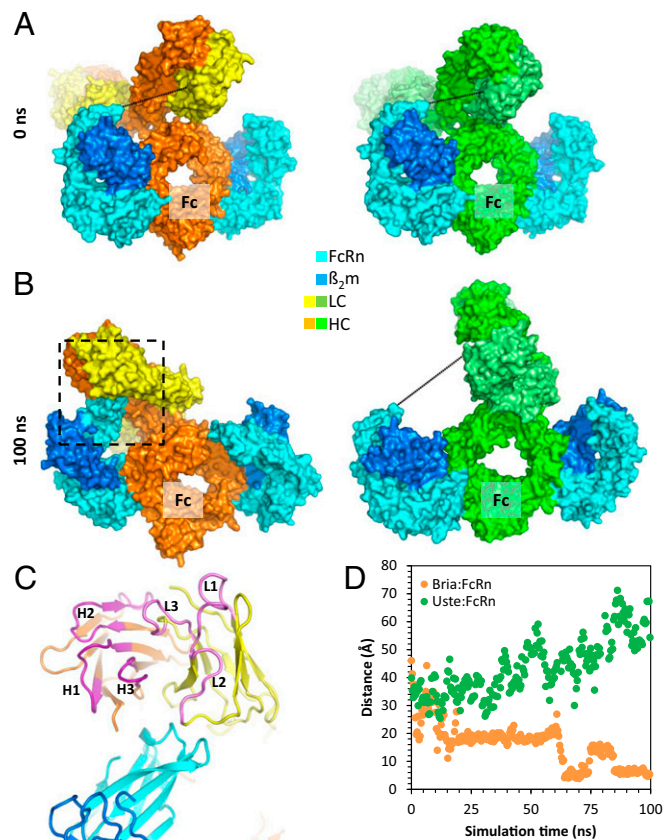

Fig. 5. Molecular dynamics simulation of FcRn–IgG models. (*A*) Conformation at the start of the simulation. The dashed line indicates the distance between two example amino acids in the Fv region and in the FcRn, which approach each other during the MD simulation as shown in *D*. The color code is identical to Fig. 1. (*B*) Conformation at the end of the simulation (*t* = 100 ns). The box indicates the part of the molecule shown in *C*. (*C*) Detailed view of the interaction between FcRn and the Fv domain of briakinumab. CDRs of the HC and the LC are colored in dark and light purple, respectively. (*D*) Distance between residues 192 (FcRn) and 57 (ustekinumab LC) and 58 (briakinumab LC), respectively, during the course of the simulation. Protein structures were prepared with PyMol (Schrodinger LLC).

Imaging was performed on a Leica SP8 confocal microscope using hybrid detectors (HyD). Imaging conditions were as follows: 100×/1.46 N.A. oil immersion lens with sequential acquisition for each channel using white light laser excitation (Ex) at 488 nm/emission (Em) 491–559 nm, Ex 594/Em 600–633 nm, and Ex 633 nm/Em 637–721 nm, respectively. Images were processed by blind deconvolution using AutoQuant X3.0.3 to improve resolution.

Pharmacokinetic Studies. B6.Cg-*Fcgrt*^tm1Dcr^ Tg(FCGRT)276Dcr mice deficient in mouse FcRn α-chain gene, but hemizygous transgenic for a human FcRn α-chain gene (mFcRn$^{-/-}$ huFcRn tg $^{+/-}$, line 276), were used for the pharmacokinetic studies (38). A single dose of antibody was injected i.v. via the lateral tail vein at a dose level of 10 mg/kg. The mice were divided into three groups of six mice each to cover nine serum collection time points in total (at 0.08, 2, 8, 24, 48, 168, 336, 504, and 672 h post-dose). Each mouse was subjected twice to retro-orbital bleeding, performed under light anesthesia with isoflurane (CP-Pharma GmbH); a third blood sample was collected at the time of euthanasia. Blood was collected into serum tubes (Microvette 500Z-Gel; Sarstedt). After 2 h incubation, samples were centrifuged for 3 min at $9,300 \times g$ to obtain serum. After centrifugation, serum samples were stored frozen at −20 °C until analysis.

Determination of Human Antibody Serum Concentrations. Concentrations of ustekinumab, briakinumab, mAb 8, and mAb 9 in murine serum were determined by specific enzyme-linked immunoassays. Biotinylated interleukin 12 and digoxigenin-labeled anti-human-Fc mouse monoclonal antibody (Roche Diagnostics) were used for capturing and detection, respectively. Streptavidin-coated microtiter plates (Roche Diagnostics) were coated with capture protein diluted in assay buffer (Universal buffer for ELISA; Roche Diagnostics) for 1 h. After washing, serum samples were added at various dilutions, followed by another incubation step for 1 h. After repeated washings, bound human antibodies were detected by subsequent incubation with detection antibody, followed by an anti-digoxigenin antibody conjugated to horseradish peroxidase (HRP) (Roche Diagnostics). ABTS (2,2′Azino-di[3-ethylbenzthiazoline sulfonate; Roche Diagnostics) was used as HRP substrate to form a colored reaction product. Absorbance of the resulting reaction product was read at 405 nm with a reference wavelength at 490 nm using a Tecan sunrise plate reader. All serum samples and positive and negative control samples were analyzed in duplicate and calibrated against a reference standard using a four-parameter fit.

1. Edelman GM (1991) Antibody structure and molecular immunology. *Scand J Immunol* 34(1):1–22.
2. Reff ME, Heard C (2001) A review of modifications to recombinant antibodies: Attempt to increase efficacy in oncology applications. *Crit Rev Oncol Hematol* 40(1):25–35.
3. Waldmann TA, Strober W (1969) Metabolism of immunoglobulins. *Prog Allergy* 13: 1–110.
4. Ghetie V, Ward ES (2000) Multiple roles for the major histocompatibility complex class I- related receptor FcRn. *Annu Rev Immunol* 18:739–766.
5. Chaudhury C, et al. (2003) The major histocompatibility complex-related Fc receptor for IgG (FcRn) binds albumin and prolongs its lifespan. *J Exp Med* 197(3):315–322.
6. Qiao SW, et al. (2008) Dependence of antibody-mediated presentation of antigen on FcRn. *Proc Natl Acad Sci USA* 105(27):9337–9342.
7. Roopenian DC, et al. (2003) The MHC class I-like IgG receptor controls perinatal IgG transport, IgG homeostasis, and fate of IgG-Fc-coupled drugs. *J Immunol* 170(7):3528–3533.
8. Simister NE, Mostov KE (1989) An Fc receptor structurally related to MHC class I antigens. *Nature* 337(6203):184–187.
9. Kuo TT, et al. (2010) Neonatal Fc receptor: From immunity to therapeutics. *J Clin Immunol* 30(6):777–789.
10. Roopenian DC, Akilesh S (2007) FcRn: The neonatal Fc receptor comes of age. *Nat Rev Immunol* 7(9):715–725.
11. Martin WL, West AP, Jr, Gan L, Bjorkman PJ (2001) Crystal structure at 2.8 A of an FcRn/heterodimeric Fc complex: Mechanism of pH-dependent binding. *Mol Cell* 7(4):867–877.
12. Goebl NA, et al. (2008) Neonatal Fc receptor mediates internalization of Fc in transfected human endothelial cells. *Mol Biol Cell* 19(12):5490–5505.
13. Kim JK, Tsen MF, Ghetie V, Ward ES (1994) Identifying amino acid residues that influence plasma clearance of murine IgG1 fragments by site-directed mutagenesis. *Eur J Immunol* 24(3):542–548.
14. Sánchez LM, Penny DM, Bjorkman PJ (1999) Stoichiometry of the interaction between the major histocompatibility complex-related Fc receptor and its Fc ligand. *Biochemistry* 38(29):9471–9476.
15. Huber AH, Kelley RF, Gastinel LN, Bjorkman PJ (1993) Crystallization and stoichiometry of binding of a complex between a rat intestinal Fc receptor and Fc. *J Mol Biol* 230(3):1077–1083.
16. Ober RJ, Martinez C, Lai X, Zhou J, Ward ES (2004) Exocytosis of IgG as mediated by the receptor, FcRn: An analysis at the single-molecule level. *Proc Natl Acad Sci USA* 101(30):11076–11081.
17. Ober RJ, Martinez C, Vaccaro C, Zhou J, Ward ES (2004) Visualizing the site and dynamics of IgG salvage by the MHC class I-related receptor, FcRn. *J Immunol* 172(4):2021–2029.
18. Akilesh S, Christianson GJ, Roopenian DC, Shaw AS (2007) Neonatal FcR expression in bone marrow-derived cells functions to protect serum IgG from catabolism. *J Immunol* 179(7):4580–4588.
19. Montoyo HP, et al. (2009) Conditional deletion of the MHC class I-related receptor FcRn reveals the sites of IgG homeostasis in mice. *Proc Natl Acad Sci USA* 106(8):2788–2793.
20. Rodewald R (1976) pH-dependent binding of immunoglobulins to intestinal cells of the neonatal rat. *J Cell Biol* 71(2):666–669.
21. Vaccaro C, Zhou J, Ober RJ, Ward ES (2005) Engineering the Fc region of immunoglobulin G to modulate in vivo antibody levels. *Nat Biotechnol* 23(10):1283–1288.
22. Suzuki T, et al. (2010) Importance of neonatal FcR in regulating the serum half-life of therapeutic proteins containing the Fc domain of human IgG1: A comparative study of the affinity of monoclonal antibodies and Fc-fusion proteins to human neonatal FcR. *J Immunol* 184(4):1968–1976.
23. Wang W, et al. (2011) Monoclonal antibodies with identical Fc sequences can bind to FcRn differentially with pharmacokinetic consequences. *Drug Metab Dispos* 39(9):1469–1477.
24. Schlothauer T, et al. (2013) Analytical FcRn affinity chromatography for functional characterization of monoclonal antibodies. *MAbs* 5(4):576–586.
25. Gandhi M, Alwawi E, Gordon KB (2010) Anti-p40 antibodies ustekinumab and briakinumab: Blockade of interleukin-12 and interleukin-23 in the treatment of psoriasis. *Semin Cutan Med Surg* 29(1):48–52.
26. Zhu Y, et al. (2009) Population pharmacokinetic modeling of ustekinumab, a human monoclonal antibody targeting IL-12/23p40, in patients with moderate to severe plaque psoriasis. *J Clin Pharmacol* 49(2):162–175.
27. Lima XT, Abuabara K, Kimball AB, Lima HC (2009) Briakinumab. *Expert Opin Biol Ther* 9(8):1107–1113.
28. Weger W (2010) Current status and new developments in the treatment of psoriasis and psoriatic arthritis with biological agents. *Br J Pharmacol* 160(4):810–820.
29. Luo J, et al. (2010) Structural basis for the dual recognition of IL-12 and IL-23 by ustekinumab. *J Mol Biol* 402(5):797–812.
30. Israelachvili JN (1985) *Intermolecular and Surface Forces* (Academic, New York).
31. Tzaban S, et al. (2009) The recycling and transcytotic pathways for IgG transport by FcRn are distinct and display an inherent polarity. *J Cell Biol* 185(4):673–684.
32. Petkova SB, et al. (2006) Enhanced half-life of genetically engineered human IgG1 antibodies in a humanized FcRn mouse model: Potential application in humorally mediated autoimmune disease. *Int Immunol* 18(12):1759–1769.
33. Dall'Acqua WF, Kiener PA, Wu H (2006) Properties of human IgG1s engineered for enhanced binding to the neonatal Fc receptor (FcRn). *J Biol Chem* 281(33):23514–23524.
34. Khawli LA, Mizokami MM, Sharifi J, Hu P, Epstein AL (2002) Pharmacokinetic characteristics and biodistribution of radioiodinated chimeric TNT-1, -2, and -3 monoclonal antibodies after chemical modification with biotin. *Cancer Biother Radiopharm* 17(4):359–370.
35. Putnam WS, Prabhu S, Zheng Y, Subramanyam M, Wang YM (2010) Pharmacokinetic, pharmacodynamic and immunogenicity comparability assessment strategies for monoclonal antibodies. *Trends Biotechnol* 28(10):509–516.
36. Igawa T, et al. (2010) Reduced elimination of IgG antibodies by engineering the variable region. *Protein Eng Des Sel* 23(5):385–392.
37. Boswell CA, et al. (2010) Effects of charge on antibody tissue distribution and pharmacokinetics. *Bioconjug Chem* 21(12):2153–2163.
38. Roopenian DC, Christianson GJ, Sproule TJ (2010) Human FcRn transgenic mice for pharmacokinetic evaluation of therapeutic antibodies. *Methods Mol Biol* 602:93–104.
39. Yeung YA, et al. (2009) Engineering human IgG1 affinity to human neonatal Fc receptor: Impact of affinity improvement on pharmacokinetics in primates. *J Immunol* 182(12):7663–7671.
40. Prabhat P, et al. (2007) Elucidation of intracellular recycling pathways leading to exocytosis of the Fc receptor, FcRn, by using multifocal plane microscopy. *Proc Natl Acad Sci USA* 104(14):5889–5894.
41. Lampson MA, Schmoranzer J, Zeigerer A, Simon SM, McGraw TE (2001) Insulin-regulated release from the endosomal recycling compartment is regulated by budding of specialized vesicles. *Mol Biol Cell* 12(11):3489–3501.
42. Gan Z, Ram S, Vaccaro C, Ober RJ, Ward ES (2009) Analyses of the recycling receptor, FcRn, in live cells reveal novel pathways for lysosomal delivery. *Traffic* 10(5):600–614.
43. Ward ES, et al. (2005) From sorting endosomes to exocytosis: Association of Rab4 and Rab11 GTPases with the Fc receptor, FcRn, during recycling. *Mol Biol Cell* 16(4):2028–2038.
44. Christianson GJ, et al. (2012) Monoclonal antibodies directed against human FcRn and their applications. *MAbs* 4(2):208–216.
45. Edelman GM, et al. (1969) The covalent structure of an entire γG immunoglobulin molecule. *Proc Natl Acad Sci USA* 63(1):78–85.